Supporting Information

Inhomogeneous Quantized Single-Electron Charging and Electrochemical-Optical Insights on Transition-Sized Atomically Precise Gold Nanoclusters

Shuang Chen, [†,‡,⊥] Tatsuya Higaki, [‖,⊥] Hedi Ma, [§,⊥] Manzhou Zhu, [†,‡] Rongchao Jin,*[,‖] and Gangli Wang*[,§]

† Institutes of Physical Science and Information Technology, Anhui University, Hefei, Anhui 230601, People's Republic of China.

‡ Key Laboratory of Structure and Functional Regulation of Hybrid Materials, Ministry of Education, Anhui University, Hefei, Anhui 230601, People's Republic of China.

§ Department of Chemistry, Georgia State University, Atlanta, Georgia 30302, United States

‖ Department of Chemistry, Carnegie Mellon University, Pittsburgh, Pennsylvania 15213, United States

⊥ These authors contribute equally.

Corresponding Authors:

*(G.W.) Email: glwang@gsu.edu.

*(R.J.) Email: rongchao@andrew.cmu.edu.

List:

Chemicals and Syntheses

Supplementary Figures and Tables

Table S1. Peak spacings of Au_{133}, Au_{144} and Au_{279} from the oxidation and reduction DPVs (Figure 3).

Table S2. The calculated peak broadening and experimental peak width at half-maximum ($W_{1/2}$) in DPV results.

Figure S1. The steady-state UV-visible absorption spectra of Au_{133}, Au_{144} and Au_{279} nanoclusters.

Figure S2. CVs of Au_{133} at 0.1, 1.0 and 2.5 V/s scan rate.

Figure S3. CVs of Au_{144} at 0.1, 1.0 and 2.5 V/s scan rate.

Figure S4. The UV-visible spectra of Au_{133}, Au_{144} and Au_{279} before and after voltammetry measurements.

Figure S5. Peak spacing of Au_{133} at 298, 232 and 195 K.

Figure S6. Peak spacing of Au_{144} at 298, 232 and 195 K.

Figure S7. The steady-state UV-visible absorption spectra of $Au_{144}(TBBM)_{60}$ and $Au_{144}(BM)_{60}$.

Figure S8. The DPVs of $Au_{144}(BM)_{60}$ and $Au_{144}(TBBM)_{60}$ nanoclusters at 298, 232 and 195 K.

Figure S9. Temperature dependence of electrochemical properties of $Au_{144}(BM)_{60}$ and $Au_{144}(TBBM)_{60}$.

Figure S10. The DPVs and ΔVs of Au_{246} at 232 and 195 K.

Figure S11. The original UV-visible absorption spectra of Au_{133} after reductive electrolysis (Figure 5).

Figure S12. The original UV-visible absorption spectra of Au_{133} after oxidative electrolysis (Figure 5).

Figure S13. The original UV-visible absorption spectra of Au_{144} after reductive electrolysis (Figure 5).

Figure S14. The original UV-visible absorption spectra of Au_{144} after oxidative electrolysis (Figure 5).

Chemicals

TetrachloroAuric (III) acid ($HAuCl_4 \cdot 3H_2O$, >99.99% metals basis, Aldrich), Tetraoctylammonium bromide (TOAB, ≥98%, Fluka), 2-Phenylethanethiol (PET, C_8H_9SH, 98%, Aldrich), L-Glutathione (GSH, reduced, 98+%, Alfa Aesar), Benzyl mercaptan (BM, C_7H_7SH, 99%, Aldrich), 4-*tert*-Butylbenzenethiol (TBBT, $C_{10}H_{13}SH$, >97.0%, TCI), Butylbenzyl mercaptan (BM, C_7H_7SH, Aldrich), P-methylthiophenol (p-MBT, C_7H_8S, 98%, Aldrich), Sodium borohydride ($NaBH_4$, Aldrich). Solvents: Methanol (MeOH, HPLC grade, ≥99.9%, Aldrich), Ethanol (EtOH, ACS reagent, ≥99.5%, Aldrich), Acetone (HPLC grade, ≥99.9%, Aldrich), Acetonitrile (ACN, HPLC grade, ≥99.9%, Aldrich), Dichloromethane (DCM, ACS reagent, ≥99.5%, Aldrich), Toluene (Tol, HPLC grade, ≥99.9%, Aldrich). All chemicals were used without further purification. Nanopure water was prepared with a Barnstead NANOpure Diamond system.

Synthesis of $Au_{133}(TBBT)_{52}$, $Au_{144}(BM)_{60}$, $Au_{144}(TBBM)_{60}$, $Au_{246}(p\text{-}MBT)_{80}$, $Au_{279}(TBBT)_{84}$ nanoclusters.

$Au_{133}(TBBT)_{52}$ was synthesized by a ligand-exchange reaction from $Au_{144}(PET)_{60}$ according to the literature procedure.[S1]

$Au_{144}(BM)_{60}$ was prepared by a ligand-exchange/size-focusing from polydispersed $Au_x(SG)_y$ based on the literature procedure with slight modification.[S2] Briefly, $HAuCl_4 \cdot 3H_2O$ (0.3 mmol, 118 mg) and L-Glutathione (GSH, 1.85 mmol, 570 mg) were dissolved in acetone (30 mL) in a 100 mL round-bottom flask. After vigorously stirring for 15 min, $NaBH_4$ (3 mmol, 114 mg dissolved freshly in 5 mL of cold Nanopure water) was rapidly added to the solution under vigorous stirring. The solution turned black immediately indicating formation of Au clusters, which then precipitated out of the acetone solution. After stirring for 1 hour, colorless supernatant was discarded and black precipitate was dissolved in 3 mL of Nanopure water. The aqueous solution of polydispersed $Au_x(SG)_y$ was transferred to a 50 mL round-bottom flask with 2 mL of toluene, 0.3 mL of ethanol and 1 ml of benzyl mercaptan. The solution was heated up to 85 ℃ for 28 hours. Then, methanol was added to the reaction mixture to precipitate the product, followed by centrifugation, and the solid product was further washed with methanol to remove excess thiol. This washing step was performed several times and finally pure $Au_{144}(BM)_{60}$ nanocluster was extracted with dichloromethane. The solvent was then evapoarted for storage and for further characterization.

$Au_{144}(TBBM)_{60}$ was prepared by a ligand-exchange reaction from $Au_{144}(PET)_{60}$ nanoclusters that are prepared according to the literature preparation.[S3] The prepared $Au_{144}(PET)_{60}$ was added into a 50 mL round-bottom flask with 1 mL toluene and 0.5 mL p-tert-butyl benzyl mercaptan. The reaction was allowed for 15 h under 80 ℃. Then, 20 mL methanol was added followed by centrifugation, and the precipitate was further washed three times with methanol. Dichloromethane was used to extract the $Au_{144}(TBBM)_{60}$ and the solution was removed by rotary evaporator for further experiments.

$Au_{246}(p\text{-}MBT)_{80}$ was synthesized following the two-step "size-focusing" method.[S4]

$Au_{279}(TBBT)_{84}$ was synthesized by a ligand-exchange reaction with TBBT using $Au_{333}(TBBM)_{79}$ prepared by a stepwise size focusing method according to the literature procedure.[S5]

Supporting References:

S1. Zeng, C.; Chen, Y.; KirschbAum, K.; Appavoo, K.; Sfeir, M. Y.; Jin, R. Structural Patterns at All Scales in a Nonmetallic Chiral $Au_{133}(SR)_{52}$ Nanoparticle. *Sci. Adv.* **2015**, *1*, e1500045.

S2. Liu, C.; Yan, C.; Lin, J.; Yu, C.; Huang, J.; Li, G. One-Pot Synthesis of $Au_{144}(SCH_2Ph)_{60}$ Nanoclusters and Their Catalytic Application. *J. Mater. Chem. A* **2015**, *3*, 20167–20173.

S3. Qian, H.; Jin, R. Ambient Synthesis of $Au_{144}(SR)_{60}$ Nanoclusters in Methanol. *Chem. Mater.* **2011**, *23*, 2209–2217.

S4. Zeng, C.; Chen, Y.; Kirschbaum, K.; Lambright, K. J.; Jin, R., Emergence of hierarchical structural complexities in nanoparticles and their assembly. *Science* **2016,** *354* (6319), 1580-1584.
S5. Higaki, T.; Zhou, M.; Lambright, K. J.; KirschbAum, K.; Sfeir, M. Y.; Jin, R. Sharp Transition from Nonmetallic Au_{246} to Metallic Au_{279} with Nascent Surface Plasmon Resonance. *J. Am. Chem. Soc.* **2018**, *140*, 5691–5695.
S6. Zhou, M.; Zeng, C.; Song, Y.; Padelford, J. W.; Wang, G.; Sfeir, M. Y.; Higaki, T.; Jin, R., On the Non-Metallicity of 2.2 nm $Au_{246}(SR)_{80}$ Nanoclusters. *Angew. Chem. Int. Ed.* **2017,** *56*, 16257-16261.

Supplementary Tables and Figures:

Table S1. Peak spacings of $Au_{133}(TBBT)_{52}$, $Au_{144}(BM)_{60}$ and $Au_{279}(TBBT)_{84}$ from the oxidation and reduction DPVs.

			R6-R7	R5-R6	R4-R5	R3-R4	R2-R3	R1-R2	R1-O1	O1-O2	O2-O3	O3-O4	O4-O5	O5-O6
Au_{133}	298 K	Ox.	-	0.24_8	0.21_2	0.19_2	0.23_2	0.22_8	0.40_0	0.24_8	0.24_4	0.23_2	0.22_8	0.20_0
		Re.	-	0.24_4	0.20_8	0.19_6	0.22_8	0.24_4	0.40_0	0.24_8	0.24_8	0.23_2	0.22_4	0.19_6
	232 K	Ox.	-	-	-	0.21_2	0.22_0	0.23_2	0.40_8	0.22_8	0.22_8	0.21_6	0.21_6	-
		Re.	-	-	-	0.20_8	0.22_4	0.23_2	0.40_8	0.22_8	0.22_8	0.21_6	0.21_6	-
	195 K	Ox.	-	-	-	0.20_4	0.23_2	0.22_4	0.40_8	0.21_6	0.21_6	0.21_2	0.21_6	0.18_8
		Re.	-	-	-	0.20_4	0.23_2	0.22_4	0.40_8	0.21_6	0.21_2	0.21_2	0.21_2	0.19_2
Au_{144}	298 K	Ox.	-	0.16_8	0.28_4	0.16_0	0.39_1	0.21_6	0.23_8	0.22_0	0.21_7	0.17_4	0.15_2	-
		Re.	-	0.16_8	0.28_4	0.16_0	0.39_2	0.21_6	0.23_8	0.22_0	0.22_0	0.17_2	0.14_8	-
	232 K	Ox.	0.17_2	0.16_8	0.28_8	0.14_8	0.41_6	0.18_6	0.22_2	0.18_4	0.20_4	0.16_0	0.16_4	-
		Re.	0.16_8	0.16_4	0.29_2	0.15_2	0.41_4	0.18_8	0.22_0	0.18_4	0.20_8	0.15_2	0.16_4	-
	195 K	Ox.	0.16_4	0.18_0	0.31_0	0.14_0	0.41_4	0.17_6	0.21_2	0.17_8	0.20_4	0.15_6	0.15_6	-
		Re.	0.16_4	0.18_0	0.30_8	0.14_0	0.41_6	0.18_0	0.20_8	0.17_6	0.21_2	0.15_2	0.15_6	-
Au_{279}	232 K	Ox.	-	-	0.14_4	0.16_8	0.16_4	0.16_4	0.17_4	0.16_6	0.16_8	0.16_4	0.13_6	-
		Re.	-	-	0.14_8	0.16_8	0.16_4	0.16_8	0.17_6	0.16_4	0.16_8	0.16_0	0.14_0	-

Table S2. The calculated peak broadening and experimental peak width at half-maximum ($W_{1/2}$) in DPV results. The experimental $W_{1/2}$ is determined from one QDL peak in the middle, i.e. the second oxidation peak (O2/O3), in a sample by using the DPV current at gap as baseline.

	Cal. $W_{1/2}$ (mV)	Exp. $W_{1/2}$ of Au_{133} (mV)	Exp. $W_{1/2}$ of Au_{144} (mV)
298 K	90.0	100.0	90.0
232 K	70.0	89.4	82.4
195 K	62.0	91.2	73.1

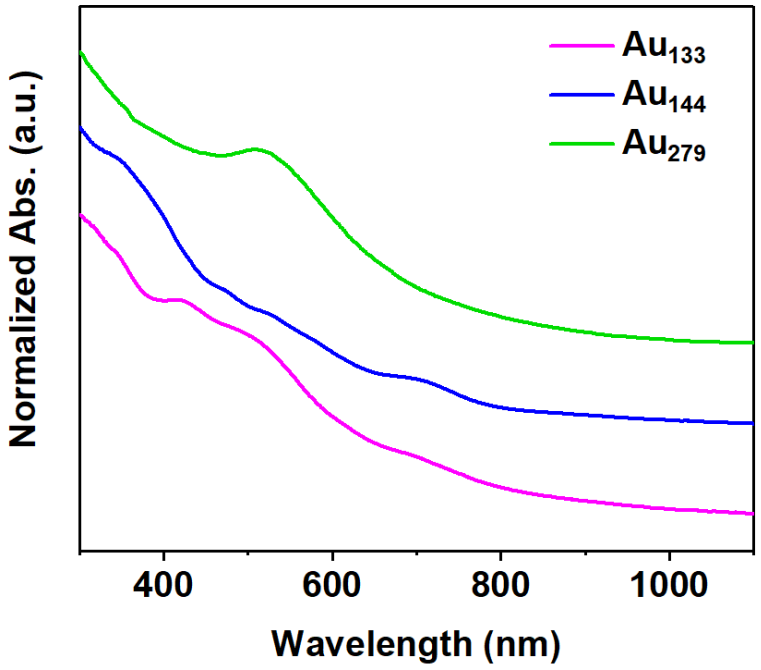

Figure S1. The steady-state UV-visible absorption spectra of Au_{133}, Au_{144} and Au_{279} nanoclusters.

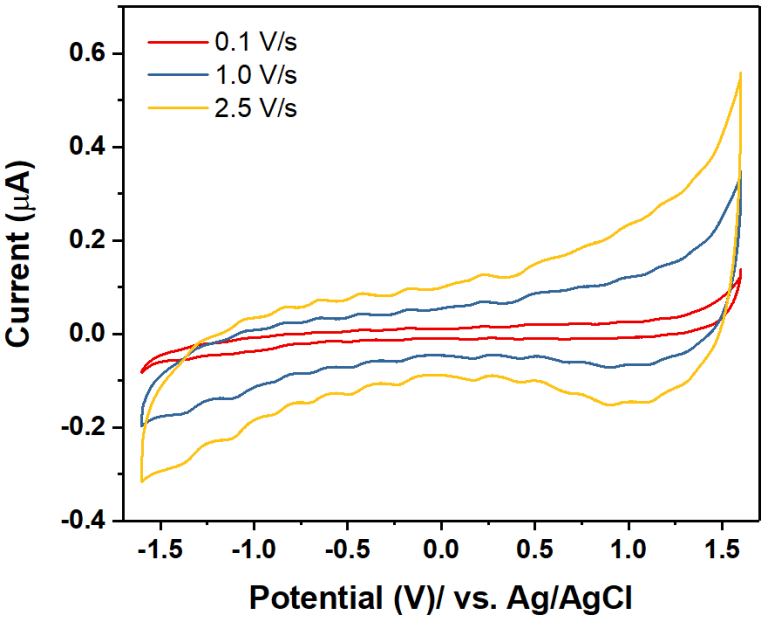

Figure S2. CVs of Au_{133} at 0.1, 1.0 and 2.5 V/s scan rate.

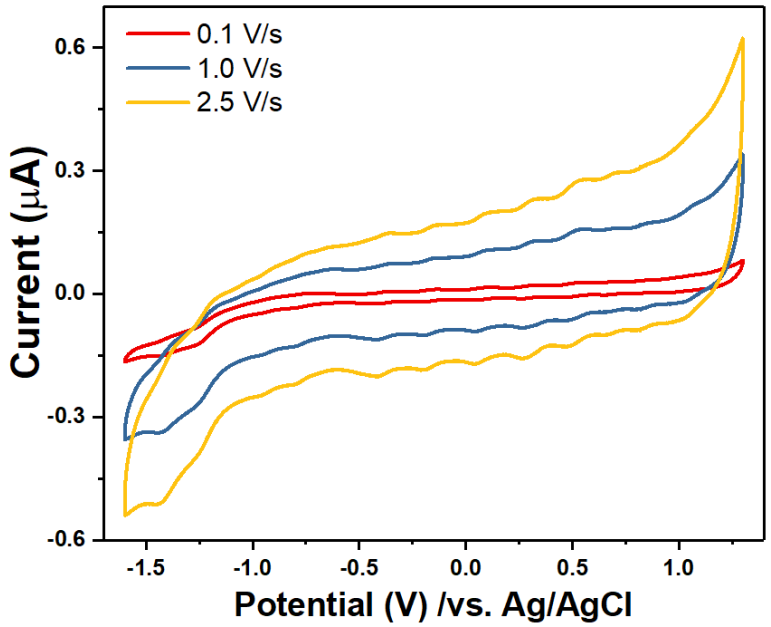

Figure S3. CVs of Au_{144} at 0.1, 1.0 and 2.5 V/s scan rate.

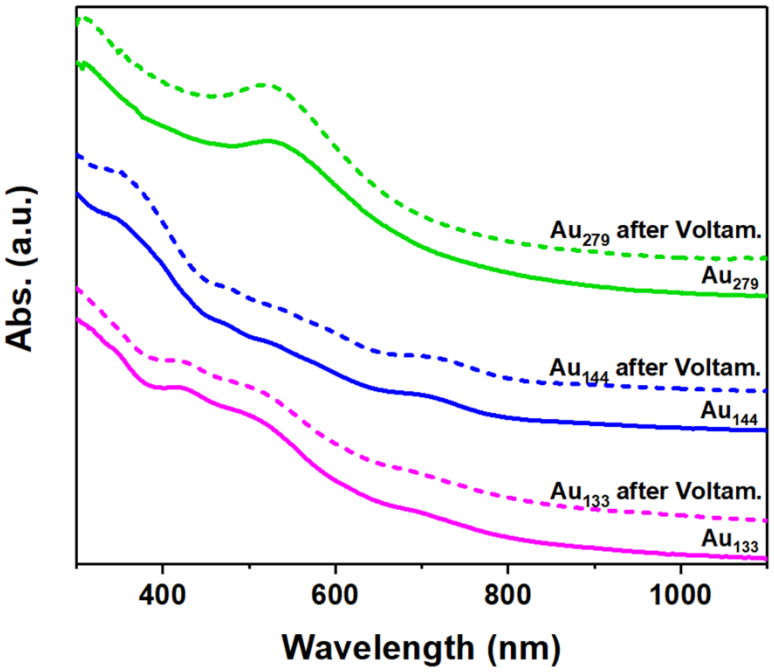

Figure S4. The UV-visible spectra of Au_{133}, Au_{144} and Au_{279} before and after voltammetry measurements. Solid lines are the original spectra, and dash lines are the spectra after measurements.

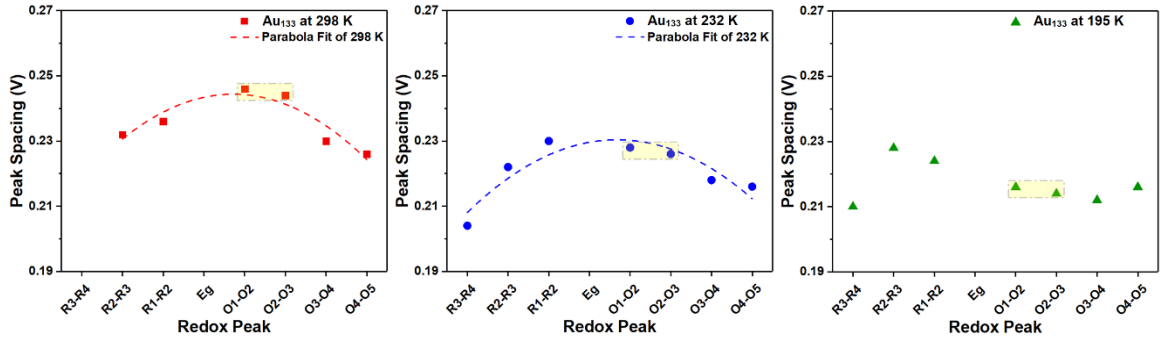

Figure S5. Peak spacing of Au_{133} at 298, 232 and 195 K. Dash lines are the fitting of ΔVs at 298 and 232 K, which display a parabolic shape. The parabolas show decreased bending radian as the temperature decrease. The data points highlighted in yellow rectangle are attributed to charging energy.

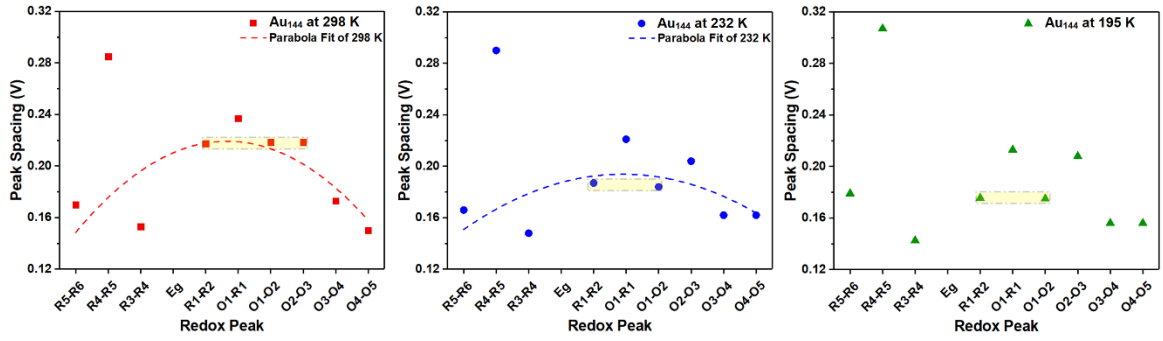

Figure S6. Peak spacing of Au_{144} at 298, 232 and 195 K. Dash lines are the fitting of ΔVs at 298 and 232 K, which display a parabolic shape. The parabolas show decreased bending radian as the temperature decrease. The data points highlighted in yellow rectangle are attributed to charging energy.

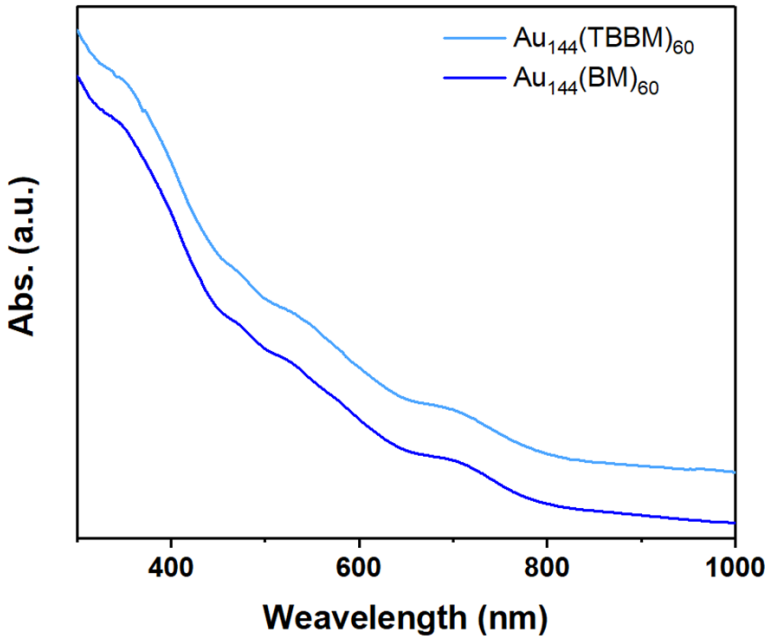

Figure S7. The steady-state UV-visible absorption spectra of $Au_{144}(TBBM)_{60}$ and $Au_{144}(BM)_{60}$ nanoclusters.

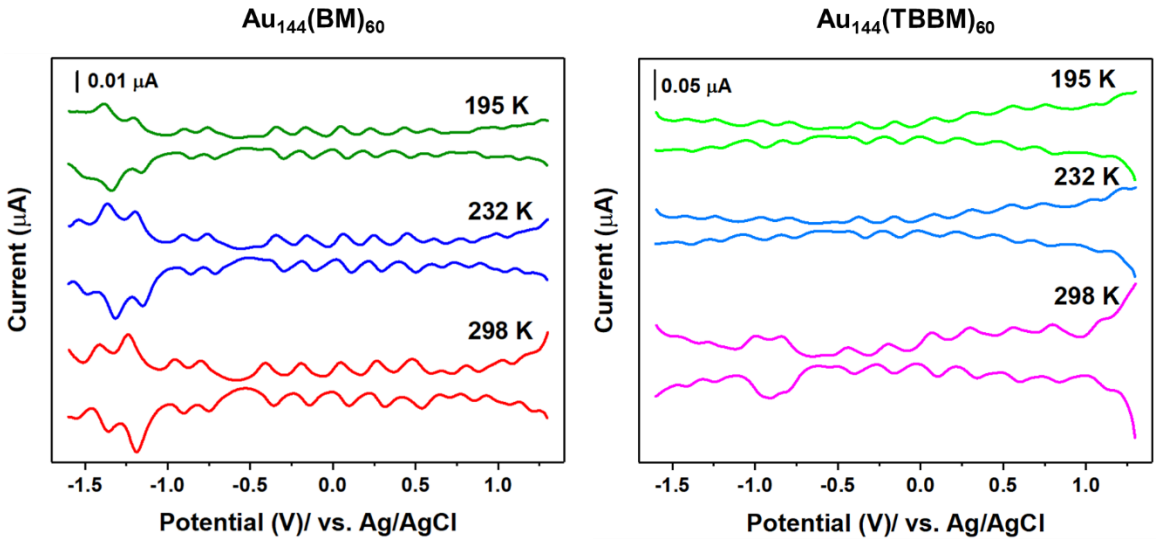

Figure S8. The DPVs of $Au_{144}(BM)_{60}$ and $Au_{144}(TBBM)_{60}$ nanoclusters at 298, 232 and 195 K.

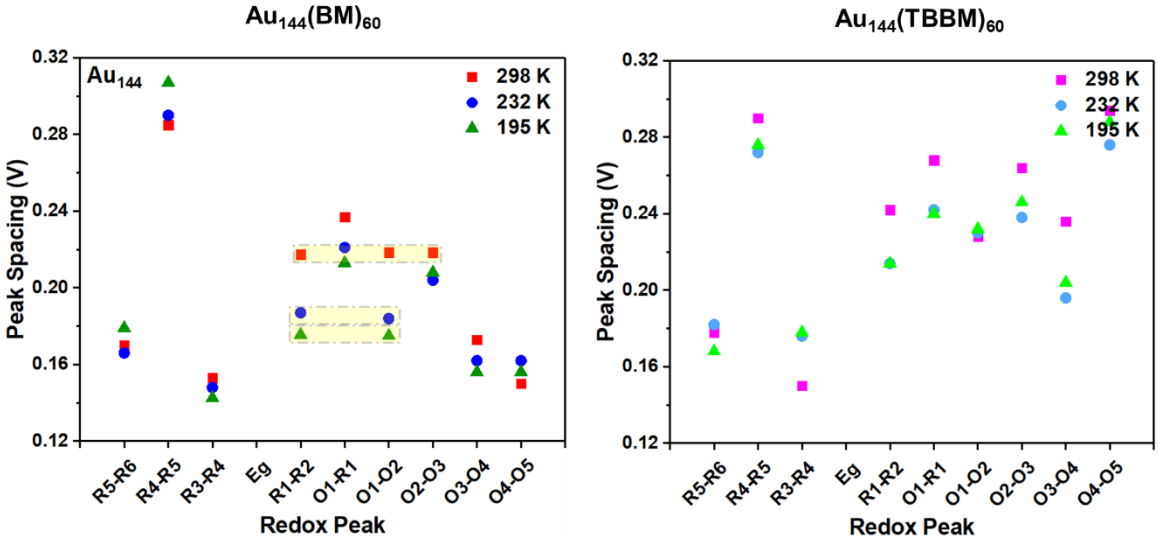

Figure S9. Peak spacing ΔVs and temperature dependence of electrochemical properties of $Au_{144}(BM)_{60}$ and $Au_{144}(TBBM)_{60}$ nanoclusters.

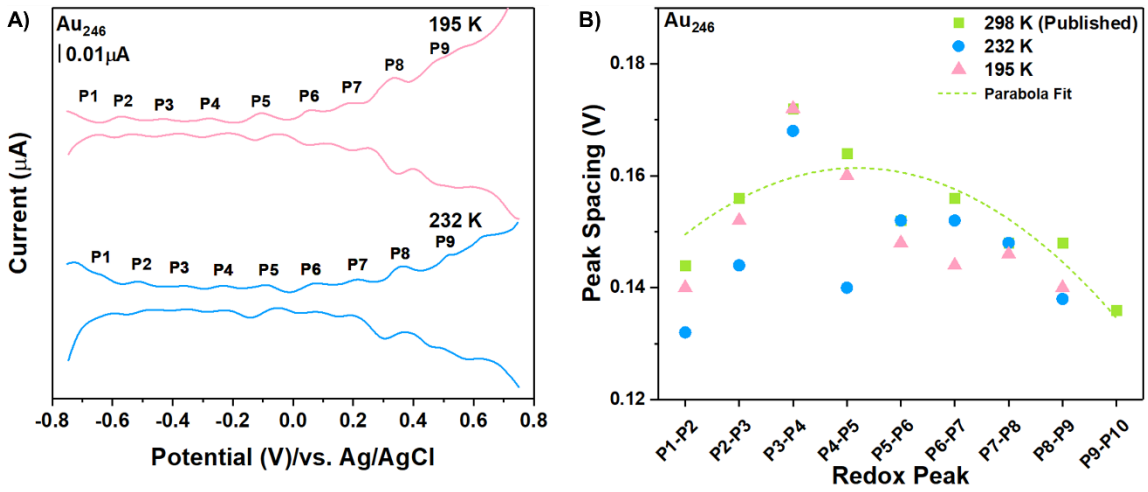

Figure S10. A) The DPVs and ΔVs of Au_{246} at 232 and 195 K. B) Analysis of peak spacing of Au_{246}. The data of peak spacing at 298 K is cited from the published literature.[S6]

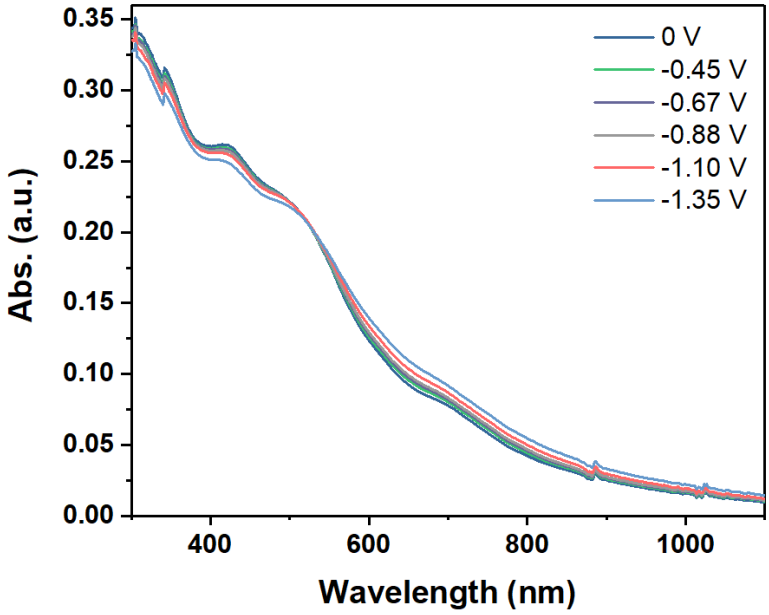

Figure S11. The original UV-visible absorption spectra of Au_{133} after reductive electrolysis (Figure 5).

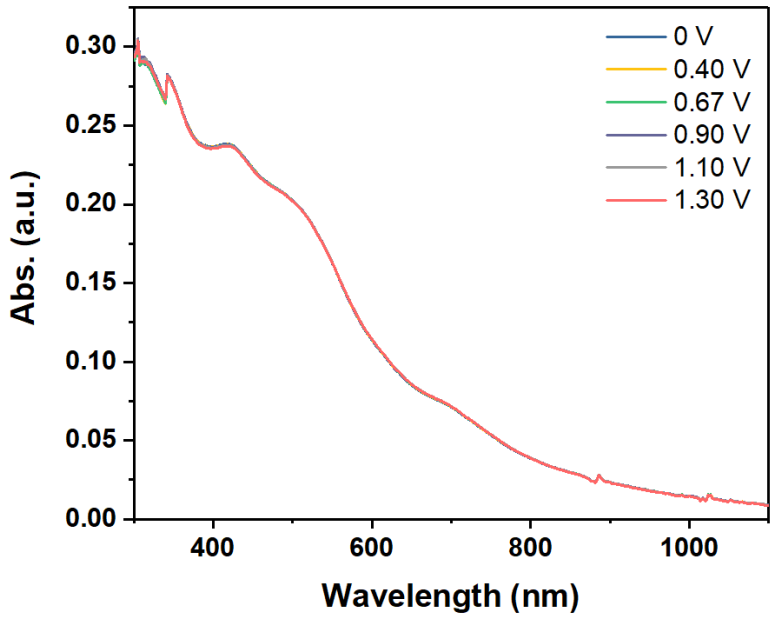

Figure S12. The original UV-visible absorption spectra of Au_{133} after oxidative electrolysis (Figure 5).

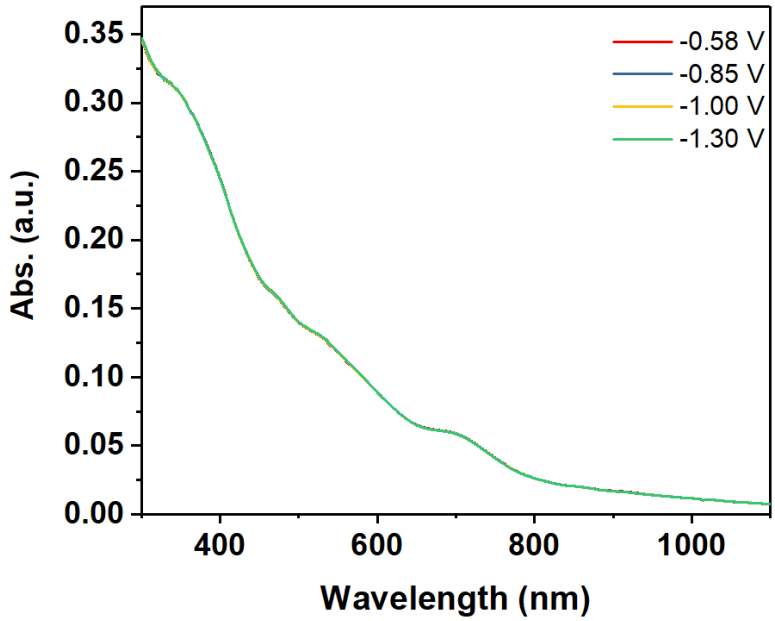

Figure S13. The original UV-visible absorption spectra of Au_{144} after reductive electrolysis (Figure 5).

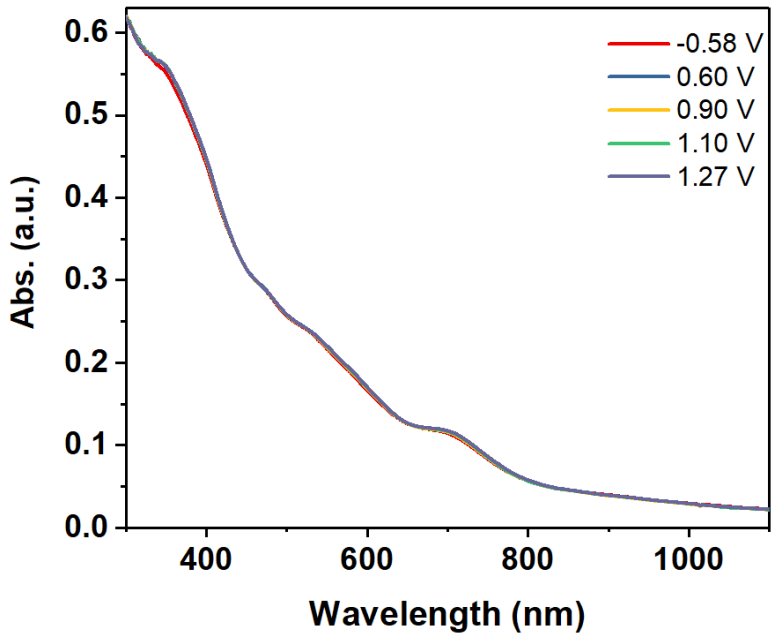

Figure S14. The original UV-visible absorption spectra of Au_{144} after oxidative electrolysis (Figure 5).